Band touching from real-space topology in frustrated hopping models

Doron L. Bergman,[1] Congjun Wu,[2] and Leon Balents[3]
[1]*Department of Physics, Yale University, New Haven, Connecticut 06520-8120, USA*
[2]*Department of Physics, University of California, San Diego, La Jolla, California 92093-0319, USA*
[3]*Kavli Institute for Theoretical Physics, University of California, Santa Barbara, California 93106-4030, USA*
(Received 4 April 2008; revised manuscript received 15 August 2008; published 10 September 2008)

We study "frustrated" hopping models, in which at least one energy band—at the maximum or minimum of the spectrum—is dispersionless. The states of the flat band(s) can be represented in a basis, which is fully localized, having support on a vanishing fraction of the system in the thermodynamic limit. In the majority of examples, a dispersive band touches the flat band(s) at a number of discrete points in momentum space. We demonstrate that this band touching is related to states which exhibit nontrivial topology in real-space. Specifically, these states have support on one-dimensional loops which wind around the entire system (with periodic boundary conditions). A counting argument is given that determines, in each case, whether there is band touching or none, in precise correspondence to the result of straightforward diagonalization. When they are present, the topological structure protects the band touchings in the sense that they can only be removed by perturbations, which *also* split the degeneracy of the flat band.

DOI: 10.1103/PhysRevB.78.125104 PACS number(s): 71.10.Fd, 71.20.−b, 71.23.An

I. INTRODUCTION

The theory of "accidental" touching of energy bands in crystals has been recognized and studied since the early days of the quantum theory of solids.[1] By accidental, one means that the touching is not required by symmetry. A spectacular example of current interest is the Dirac point degeneracy of graphene, which leads to a host of interesting behavior.[2] Another class of heavily studied theoretical examples are the Dirac points appearing in problems of two-dimensional (2D) electrons moving in periodic potentials in a magnetic field studied by Hofstadter[3] and others. Three-dimensional (3D) Dirac points occur in models of unusual "spin Hall insulators" occurring with strong spin-orbit interactions.[4] In all these cases, despite the accidental nature of the band touching, it is robust to perturbations of the Hamiltonian. This robustness has its origin in *momentum-space topology* of the Bloch wave functions.[5] For instance, in graphene, each Dirac point is a source of a $\pm\pi$ delta-function flux of Berry curvature, so that the line integral of the Berry connection $\oint_{\mathcal{C}} d\vec{k}\cdot \mathrm{Im}\langle u_{nk}|\vec{\nabla}_k|u_{nk}\rangle = \pm\pi$ for any curve $\mathcal{C}$ enclosing a Dirac point. If time reversal and inversion symmetries are maintained, the Berry curvature vanishes identically except at points of band crossing and conservation of its flux protects the band crossings comprising the Dirac points.

In this paper, we describe the topological protection behind a completely different instance of accidental band touching, which occurs in a broad class of "frustrated" hopping models. The models which we will consider actually display, in addition to band crossings, a more dramatic phenomenon—the presence of one or more *completely flat bands*. Models with flat bands are particularly interesting physically because in this case the effect of interactions is wholly nonperturbative—interactions can reconstruct the states within the flat-band manifold without any cost in kinetic energy. This is a powerful mechanism for generating complex and interesting many-body states as attested by the richness of the fractional quantum Hall effect, which occurs as a result of the flat-band degeneracy of Landau levels of electrons in a magnetic field.

The frustrated hopping models we consider here arise in other contexts, e.g., the description of magnons in frustrated quantum antiferromagnets and the motion of cold atoms in *p*-wave Bloch-band optical lattices (in addition, flat-band electronic models have been invoked theoretically as models with exact ferromagnetic ground states[6–9]). The distinguishing feature of a flat band is that one can construct single-particle Wannier states (superpositions of wave functions with all momenta) which are strictly localized, i.e., have support on only a small finite number of sites. While Wannier states may always be constructed, only for the case of a flat band they do remain one-particle eigenstates.

In the vast majority of frustrated hopping models (we will catalog many below), the flat band is found to touch one of the dispersive bands at specific points in momentum space. We study in each case whether this band touching can be removed by some small changes in the Hamiltonian or whether it somehow enjoys protection that makes a search for such perturbations fruitless. The result of this paper is that in many cases the crossing is protected and can only be removed by perturbations that also destroy the flatness of the low-energy band. Like the protection of the Dirac points of graphene and others discussed above, the mechanism for this stability is topological. However, because of the localized character of the states in the flat band, the topological structure lies in *real-space* rather than momentum space. Specifically, the band touchings can be associated with eigenstates whose support is extended along *noncontractible loops* crossing a (toroidal) sample with periodic boundary conditions.

The remainder of this paper is organized as follows. In Sec. II, we describe in detail the structure of local and topological loop states for one of our simplest examples, the nearest-neighbor hopping model on a kagome lattice. We show how counting of these states requires band touching. In Sec. III, we give a more abbreviated presentation of the generalization of these arguments to various other frustrated lattices. Finally, we conclude with a discussion in Sec. IV.

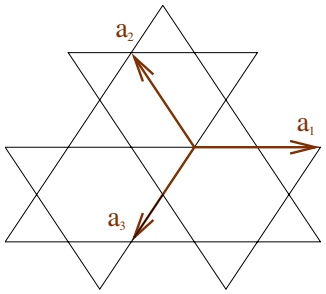

FIG. 1. (Color online) Conventions for the shortest length Bravais lattice vectors for the kagome lattice (brown arrows).

II. KAGOME LATTICE MODEL

The simplest model we will consider is the nearest-neighbor tight-hopping Hamiltonian on the kagome lattice,[6,10–13]

$$\mathcal{H}_t = -t\sum_{\langle ij\rangle}(c_i^\dagger c_j + \text{H.c.}), \tag{1}$$

where the indices i,j denote the sites of the kagome lattice and $\langle ij\rangle$ denotes nearest-neighbor pairs of sites. The particles can be either fermions or bosons. We use this simple model to demonstrate all the generic flat-band features discussed above. Aside from providing concrete examples for all the unique features of flat bands, the analysis of the kagome model also proves a good model with which to develop the techniques we will use throughout this paper.

A. Band structure

The band structure of Eq. (1) consists of a single flat band with energy $\epsilon_0(\mathbf{q})=2t$ and two dispersive bands with

$$\epsilon_\pm(\mathbf{q}) = -t(1 \pm \sqrt{3+2\Lambda(\mathbf{q})}), \tag{2}$$

where

$$\Lambda(\mathbf{q}) = \cos(\mathbf{q}\cdot\mathbf{a}_1) + \cos(\mathbf{q}\cdot\mathbf{a}_2) + \cos(\mathbf{q}\cdot\mathbf{a}_3). \tag{3}$$

Here $\mathbf{a}_{1,2,3}$ are the three shortest Bravais lattice vectors for the kagome (and triangular) lattice. The convention we use for the three vectors illustrated in Fig. 1 is $a_1=\hat{x}$, $a_2=-\frac{1}{2}\hat{x}+\frac{\sqrt{3}}{2}\hat{y}$, and $a_3=-\frac{1}{2}\hat{x}-\frac{\sqrt{3}}{2}\hat{y}$. The upper dispersive band $\epsilon_-(\mathbf{q})$ touches the flat band at the Γ point $\mathbf{q}=0$.

The hopping term in the band basis is of the form

$$\mathcal{H}_t = \sum_\nu \int_{\mathbf{q}} a_\nu^\dagger(\mathbf{q}) a_\nu(\mathbf{q})\epsilon_\nu(\mathbf{q}), \tag{4}$$

where the momentum integration is over the first Brillouin zone and we use $\nu=0,\pm$ for the band index and $\mu=1,2,3$ for the basis index. Another set of operators $a_\nu(\mathbf{q})$ are related to the original operators by a unitary transformation. In particular, momentum eigenstates of the flat band consist of

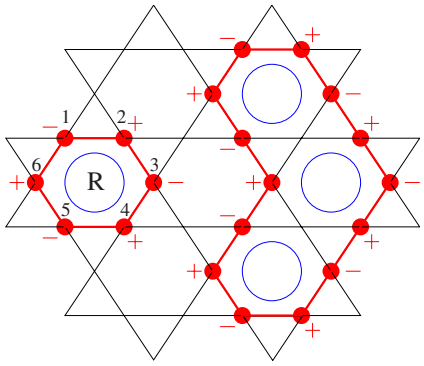

FIG. 2. (Color online) Depiction of localized eigenstates on the boundary of a single and triple plaquette. Those sites with nonzero weight are denoted by a full (red) circle. The magnitude of the weights is always the same but the phases alternate between ± 1. The phases are denoted by $\pm$ signs next to the relevant lattice sites.

$$a_0(\mathbf{q}) = \sum_{\mu=1}^{3} \psi_\mu^*(\mathbf{q}) c_\mu(\mathbf{q}) \tag{5}$$

with $\psi_\mu(\mathbf{q})=\sin(\mathbf{q}\cdot\mathbf{a}_{\mu+2}/2)/\sqrt{[3-\Lambda(\mathbf{q})]/2}$, where the Greek index arithmetic is always modulo 3 and $[3-\Lambda(\mathbf{q})]/2 = \Sigma_{\mu=1}^3 \sin^2(\mathbf{q}\cdot\mathbf{a}_{\mu+2}/2)$.

B. Localized states

We can construct localized eigenstates by taking the linear combinations

$$A_{\mathbf{R}}^\dagger = \mathcal{N}\int_{\mathbf{q}} e^{-i\mathbf{q}\cdot\mathbf{R}} a_0^\dagger(\mathbf{q})\sqrt{[3-\Lambda(\mathbf{q})]/2}, \tag{6}$$

with $\mathcal{N}$ being some normalization. Here and elsewhere we will use $A_{\mathbf{R}}^\dagger$ to denote the creation operator for the localized eigenstates. Choosing $\mathbf{R}$ to be the position at the center of a hexagonal plaquette of the lattice and normalizing the operator, we find

$$A_{\mathbf{R}}^\dagger = \frac{1}{\sqrt{6}}\sum_{j=1}^{6}(-1)^j c_j^\dagger, \tag{7}$$

where the indices $1\ldots6$ enumerate the six successive sites around the hexagonal plaquette as illustrated in Fig. 2. These local operators are very useful, but they are unfortunately *not* canonical bosons or fermions. Rather, if c_j are bosonic, the commutation relations are

$$[A_{\mathbf{R}}, A_{\mathbf{R}'}^\dagger] = \delta_{\mathbf{R},\mathbf{R}'} - \frac{1}{6}\Gamma_{\mathbf{R},\mathbf{R}'}, \tag{8}$$

where the matrix $\Gamma_{\mathbf{R},\mathbf{R}'}$ is the adjacency matrix of the *triangular* lattice formed by the centers of the plaquettes. For fermions, Eq. (8) holds with the commutator replaced by an anticommutator.

The localized model can be understood directly in real-space by considering a single triangle around the boundary of the plaquette. One of the corners has an amplitude of $\frac{1}{\sqrt{6}}$, a second has $\frac{-1}{\sqrt{6}}$, and a third has zero amplitude. The hopping

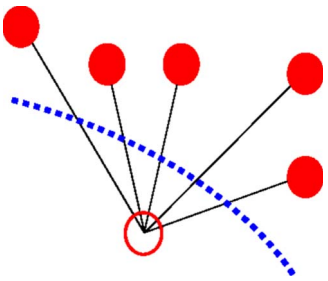

FIG. 3. (Color online) The localized states are exact eigenstates due to destructive interference between the hopping amplitudes from sites with nonzero weight (filled circles) to sites outside the boundary (empty circle). The lattice sites with nonzero weight are contained in a finite area within a boundary marked by the dashed line.

amplitude from the first and second sites onto the third site *cancels* out. Thus the eigenstate is localized as a result of *destructive interference*, which is a very useful guiding principle in identifying these states in other flat-band models. For a strictly localized wave function to be an eigenstate, the sum of hopping amplitudes onto sites outside the support of the wave function must vanish (see, for illustration, Fig. 3).

One can create similar exact single-particle eigenstates on larger loops by summing over the plaquette states on a number of contiguous plaquettes and normalizing the state by the length of the boundary of the area covered by the plaquettes

$$A^\dagger_{\partial\mathcal{A}} = \sum_{\mathbf{R}\in\mathcal{A}} A^\dagger_{\mathbf{R}} \frac{\sqrt{6}}{\sqrt{|\partial\mathcal{A}|}}. \tag{9}$$

Here $\mathcal{A}$ denotes the area covered by the plaquettes and $|\partial\mathcal{A}|$ denotes the length of the boundary of this area. In Fig. 2 we show one example of a three-plaquette loop.

C. State counting and band touching

We now turn to the main question addressed in this paper—the origin of the band touching. We will show that the set of localized eigenstates contains too many states to fit into the flat band alone. Specifically, the dimension of the space of localized state with the *energy* of the flat band has a dimension which is 1 larger than that of the flat band. This requires a contribution from a state of another band which, since it is continuous, must touch the flat band at one point.

Because the difference in question involves only a finite number of basis states (here 1, but there may be more in other examples in Sec. III), it is necessary to consider a large but finite system to make this counting precise (this counting of states was mentioned in Refs. 11 and 13 but ignored in the thermodynamic limit). It is advantageous to use periodic boundary conditions (with a finite integral number of unit cells in each of two directions), since in this case the Bloch states in Eq. (5) remain eigenstates (with discrete q) in the finite system. We must count carefully the number of linearly independent states with energy ϵ_0. The plaquette states created by Eq. (7) naively all seem linearly independent since they occur on different plaquettes. With open boundary conditions, the sum over all the plaquettes in the lattice leads to a state of the form of Eq. (9) at the boundary of the system. For periodic boundary conditions (putting the lattice on a torus), however, this sum *vanishes* since there is no boundary, $A^\dagger_{\mathbf{q}=0}=\Sigma_{\mathbf{R}}A^\dagger_{\mathbf{R}}=0$. So when considering the Hilbert space spanned by the plaquette states (7) we have only $(N-1)$ independent states, where N is the number of plaquettes (and unit cells) in the lattice. This accounts for all but one state of the flat band.

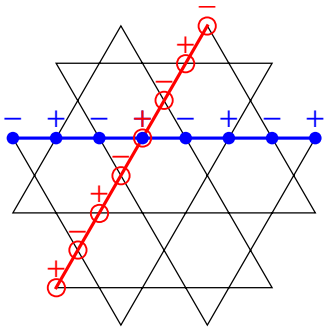

FIG. 4. (Color online) The two noncontractible loop states around the handles of the torus. One loop consists of the sites marked by full (blue) circles and the other by the empty (red) circles. As the other eigenstates in the flat band, the wave function has an alternating ± phase on the sites along the loops.

The missing state is accounted for by a noncontractible loop around the torus. By decorating such a loop with alternating plus/minus signs, as illustrated in Fig. 4, one again satisfies the conditions for destructive interference of outgoing waves, and the associated wave function represents an exact eigenstate with the flat-band energy. This state cannot be expressed as a sum of plaquette operators, or it would be possible to contract the loop just as any sum of plaquette states is. We have therefore found the missing state. However, we have an embarrassment of riches—there is not one such noncontractible loop, but *two*. In total we have $(N+1)$ states, all with the *same* energy. From the band structure we know the flat band contains precisely N states, and so the additional state must come from another band. For this reason, one of the dispersive bands touches the flat band at exactly one point.

In fact, from the loop states we can construct the plane-wave Bloch state which touches the flat band explicitly. By taking an equal weight linear superposition of the noncontractible loops translated in any direction other than that along which the loop runs, one obtains a state with the same configuration in any unit cell, which therefore has the Bloch form with momentum $\mathbf{q}=0$. The double degeneracy of states with $\mathbf{q}=0$ signifies that not only must one of the dispersing bands touch the flat band at a point, but that point is at $\mathbf{q}=0$.

III. LOCAL EIGENSTATES

A. Pyrochlore lattice model

Taking the nearest-neighbor hopping model (1) on the pyrochlore lattice (instead of the kagome lattice) has two degenerate flat bands at $\epsilon_0=2t$ and two dispersive bands

$$\epsilon_{\pm} = -2t[1 \pm \sqrt{1+\cos(q_1/2)\cos(q_2/2)+\cos(q_2/2)\cos(q_3/2)+\cos(q_3/2)\cos(q_1/2)}\,]$$

, where we have used the conventions $\mathbf{a}_1=\frac{1}{2}(0,1,1)$, $\mathbf{a}_2=\frac{1}{2}(0,1,1)$, and $\mathbf{a}_3=\frac{1}{2}(0,1,1)$ for the (fcc) Bravais lattice vectors and $\mathbf{e}_0=\frac{1}{8}(1,1,1)$, $\mathbf{e}_1=\frac{1}{8}(-1,1,1)$, $\mathbf{e}_2=\frac{1}{8}(1,-1,1)$, and $\mathbf{e}_3=\frac{1}{8}(1,1,-1)$ for the pyrochlore basis. Both flat bands touch the upper dispersive band at $\mathbf{q}=0$. The same localized plaquette modes that appear in the kagome model are exact eigenstates for this pyrochlore model as well.[13,14] However, whereas the number of hexagonal plaquettes in the kagome lattice is equal the number of unit cells, in the pyrochlore lattice the number of plaquettes is four times that of the number of unit cells. With two flat bands containing only $2N$ states, clearly these are not all linearly independent.

Consider a volume enclosed by four plaquettes (see Fig. 5). Placing plaquette states with equal weight, and appropriate relative signs, on each one of these four faces gives a total of *zero*. There are $2N$ such cells in the pyrochlore lattice and therefore $2N$ such constraints. This reduces the number of independent states we can construct out of the plaquette states to $2N$. We choose to keep all the plaquette states for the plaquettes perpendicular to two out of the four $\langle 111\rangle$ directions of the pyrochlore lattice.

Now if we consider any one of the kagome planes along the two directions we chose above, we have the same additional constraint as in the kagome lattice—putting a plaquette state on every plaquette in the plane with periodic boundary conditions results in zero, giving us one additional constraint. Taking into account the cell constraints from the previous paragraph, there are only two such linearly independent planes, so we have two additional constraints reducing the number of linearly independent states we can construct from the plaquette states to $2N-2$. As in the kagome lattice, we now have the noncontractible loop states to consider. In the pyrochlore lattice there will be three such noncontractible loops rather than two. Therefore, in total, we have $2N+1$ states with the same energy of the flat bands. Exactly as argued in the kagome case, these particular noncontractible loop states can be made into $\mathbf{q}=0$ states and we therefore have three degenerate states at $\mathbf{q}=0$. The only way for the band structure to comply with this is to have one of the dispersive bands touch the two flat bands at the $\mathbf{q}=0$ point, which indeed is the case.

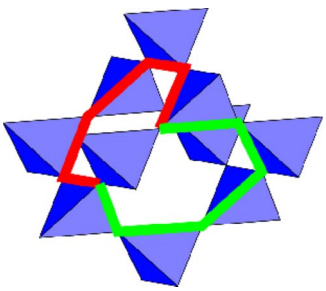

FIG. 5. (Color online) Pyrochlore volume enclosed by four plaquettes. Two of the four plaquettes are highlighted by thick (red and green) lines. Each one of the two plaquettes supports a localized eigenstate.

B. Dice lattice model

The nearest-neighbor hopping model can give rise to a flat band on other lattices as well. We considered one example of a 2D lattice and one example of a 3D lattice. In this subsection we shall mention one additional 2D lattice—the dice lattice, for a number of reasons. First, as opposed to the kagome and pyrochlore lattices, in this model the flat band touches dispersive bands at momenta other than $\mathbf{q}=0$. Second, it will be useful to compare two different models on this lattice, that will both produce a flat band. The analysis essentially follows the same steps as in the kagome lattice model, and so we will not elaborate how the results were obtained.

The dice lattice has a basis of three sites, two of which have a coordination number 3 and one with a coordination number 6. In what follows, we shall refer to the latter sites as the coordination-6 sites. On the dice lattice, the nearest-neighbor hopping model has one flat band at $\epsilon=0$ touching two dispersive bands $\epsilon_{\pm}=\pm 2t\sqrt{2}\sqrt{3+2\Lambda(\mathbf{q})}$ (with $\Lambda(\mathbf{q})$ the same as defined in Sec. I) at the two momentum points $\mathbf{q}=\pm(4\pi/\sqrt{3},0)$ (with the Bravais lattice vectors taken with length 1). Adding an on-site potential, which does not break the symmetries of the lattice (for instance an energy cost V to be on a coordination-6 site), one can gap one of the two dispersive bands away from the flat band and only two degenerate points will remain. Therefore, our counting arguments will have accounted for $N+2$ states with the energy of the flat band.

The localized eigenstates of the dice lattice model are different from those of the kagome and pyrochlore lattices. Rather than residing in a loop around one or a number of plaquettes, the simplest localized states here have nonzero weight on the six sites neighboring a central coordination-6 site with alternating signs as illustrated in Fig. 6.

As for the kagome and pyrochlore lattices, a sum over all the localized states surrounding every six-coordinated site can produce zero with periodic boundary conditions $A^{\dagger}_{\mathbf{q}=\pm(4\pi/3,0)}=\Sigma_{\mathbf{R}}e^{+i\mathbf{q}\cdot\mathbf{R}}A^{\dagger}_{\mathbf{R}}=0$. Apart from these two constraints, the localized states are all independent. The number of coordination-6 sites on the lattice is the same as the number of unit cells, and so we have accounted for $N-2$ states. As in the kagome and pyrochlore models, we will find eigenstates composed of noncontractible loops around the torus.

In Fig. 6 we show one of the two nontrivial loop states, which exist for this model, with the weights being integer powers of the factor $\omega=e^{\pm i(4\pi/3)}$ for a total of four noncontractible loop states. These are exact eigenstates provided that $1+\omega+\omega^2=0$ is satisfied. Indeed, $\omega=e^{\pm i(4\pi/3)}$ are the two solutions of this equation.

C. Honeycomb lattice *p*-band model

Another hopping model with flat bands is the *p*-band hopping model on the honeycomb lattice introduced in Ref. 15.

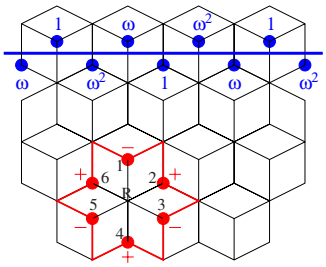

FIG. 6. (Color online) Dice lattice localized eigenstate denoted by thick (red) closed loop surrounding the site labeled by R. One of two nontrivial loops is indicated by a thick straight (blue) line. All sites with some particle weight on them are indicated by a filled circle. The amplitude is indicated on every site with nonzero weight. From this picture we can understand why the localized states are eigenstates, again invoking the picture of destructive interference. Consider the sites marked 1 and 2. Hopping from these sites can occur to either **R** or the site right outside the boundary of the localized state. in both cases, the hopping amplitude from sites 1 and 2 cancels out. Similar considerations for the other sites of the localized states yield the same result. For the noncontractible loop state, every site neighboring the sites with nonzero weight has three hopping amplitudes contributing $1+\omega+\omega^2$. As long as this sum vanishes, this is an exact eigenstate.

In this model, only the planar $p_{x,y}$ orbital states are considered at each lattice site. It is convenient to describe any superposition of the two orbital states on a site with an orbital unit vector $\vec{p}=(p_x,p_y)$ representing the state $|\vec{p}\rangle=\cos\phi|p_x\rangle+\sin\phi|p_y\rangle$ with ϕ as the angle between the arrow and the x axis. The hopping is assumed to occur only between orbital states with the orbital vector parallel to the link. The resultant tight-binding Hamiltonian is $\mathcal{H}=t\Sigma_{\langle ij\rangle}[\vec{p}_i^{\dagger}\cdot(\mathbf{r}_i-\mathbf{r}_j)][\vec{p}_j\cdot(\mathbf{r}_i-\mathbf{r}_j)]+\text{H.c}$, where the nearest-neighbor distance is taken as unity and $\vec{p}_j^{\dagger}$ ($\vec{p}_j$) are the creation (annihilation) operators for a particle at site j in the orbital state $|\vec{p}\rangle$.

The two particle-hole symmetric flat bands in this model touch dispersive bands at $\mathbf{q}=0$. For the low-energy flat band, the local eigenstates are illustrated in Fig. 7 where the arrows denote the orbital state vectors. The high-energy flat-band states have all the orbital arrows pointing in the opposite direction on *one sublattice*, $\vec{p}\rightarrow-\vec{p}$.

Exactly as for the kagome and pyrochlore lattice models, summing the localized states on all plaquettes results in zero, $a^{\dagger}_{\mathbf{q}=0}=\Sigma_{\mathbf{R}}a^{\dagger}_{\mathbf{R}}=0$. The localized states produce $N-1$ linearly independent states, leaving one state in each flat band unaccounted for. Two noncontractible loop states exist (one on each handle of the torus) with the same energy as the flat-band states, their details are illustrated in Fig. 7. A superposition of all the translations of a noncontractible loop state results in a $\mathbf{q}=0$ state. The two additional states then account for two $\mathbf{q}=0$ modes in the band structure and explain why the dispersive bands must touch the flat bands at this momentum point.

D. Dice lattice *p*-band model

Another model that can be analyzed in a similar manner is the same p-band hopping introduced in Ref. 15 on the dice lattice. This model is different from the others presented here in that the flat bands are *separated* from all the dispersive bands by finite-energy gaps. We will use the same framework to understand why the flat bands are gapped in this case.

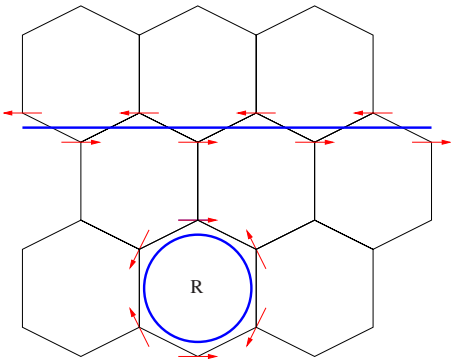

FIG. 7. (Color online) p-band honeycomb local eigenstate and noncontractible loop state. The orbital states are denoted by a vector (in the present case the vector coordinates can be chosen real). The orbital vectors are always perpendicular to one link emanating from the site and with the special form of hopping assumed in the model. The hopping amplitude on this link vanishes in this state.

The band structure for this hopping model has two degenerate flat bands at $\epsilon=0$ and two pairs of particle-hole symmetric bands with energies

$$\epsilon(\mathbf{q}) = \pm t\sqrt{2}\sqrt{(6+A)\pm\sqrt{2(2A^2-3A-3B)}}, \qquad (10)$$

with

$$A=\sum_{\mu=1}^{3}\cos(\mathbf{q}\cdot\mathbf{a}_{\mu}),$$

$$B=\sum_{\mu=1}^{3}\cos[\mathbf{q}\cdot(\mathbf{a}_{\mu}+2\mathbf{a}_{\mu+1})], \qquad (11)$$

where the three vectors $\mathbf{a}_{1,2,3}$ are the same minimal length Bravais lattice vectors indicated in Fig. 1 (now with length $\sqrt{3}$), making A,B two functions that are invariant under the full symmetry group of the model. The dispersive bands are separated from the flat bands by a gap of $\Delta=\sqrt{2}t$.

Two local eigenstate modes can be found on the same area unit surrounding a coordination-6 site. They are illustrated in Fig. 8 (type I) and Fig. 9 (type II) using the same conventions we have introduced for the honeycomb p-band model in Sec. III C. Note that the arrows indicating the orbital state are always in one of six discrete directions with the angles 0°, ±60°, ±120°, and 180° from the x-axis direction. In these states, the arrow directions are always perpendicular to one link emanating from the site.

Naively, all these states (types I and II) on different area units are linearly independent, resulting in $2N$ states that exhaust the number of states in the flat bands. However, as with the previous models explored in this paper, we will find a number of constraints that show that this is not the case.

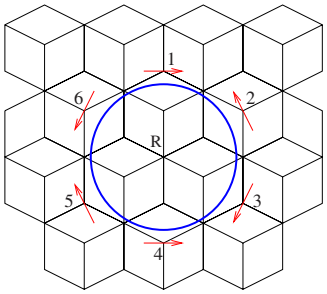

FIG. 8. (Color online) Type I p-band dice lattice local eigenstate.

Summing over the type I states on a set of nonoverlapping area units that cover the entire plane results in zero when we have periodic boundary conditions. An appropriate choice of the area units to sum over is illustrated in Fig. 10. However, there are four such distinct sets covering the entire plane and so there are four different sums (involving different sets of states) giving zero. The four sets of type I states are related by the Bravais translations of the lattice.

As in the other models we have discussed, noncontractible loop eigenstates can be constructed as illustrated in Fig. 11. The noncontractible loop eigenstates always come in pairs—one around each nontrivial loop on the torus. However, there are four pairs of distinct such states related by translation. The quadrupling is closely related to the four different unit area sets covering the plane discussed in the previous paragraph. The noncontractible loop states we are presenting here always lie on the edges of one of the four sets of area units.

There are four additional constraints involving sums over type II localized eigenstates and the noncontractible loop states. Adding the type II states on every area unit on an infinite length strip, comprising a noncontractible loop around the torus, we find the resultant state depicted in Fig. 12. The resultant state is a sum of four noncontractible loop states, of the kind depicted in Fig. 11, and so the type II states and the noncontractible loops are not linearly independent. The sum of type II on a strip translated by one Bravais lattice vector perpendicular to the strip gives another independent relation between the type II states and the noncontractible loop states. Finally, for strips around the other handle on the torus, we find two additional such relations.

In total, we have $2N$ localized eigenstates, eight noncontractible loop states, and $4+4=8$ vanishing linear combinations of these $2N+8$ states. We therefore have precisely $2N$ linearly independent states, all with the same energy of the flat bands, exhausting the number of states in the flat bands. Since no extra states at this energy need to be accounted for by the dispersive bands, a gap can occur in principle and indeed shows up in practice.

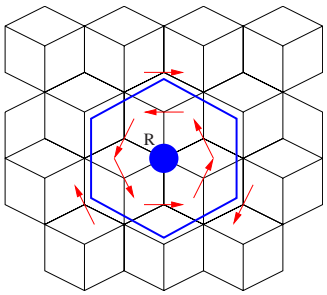

FIG. 9. (Color online) Type II p-band dice lattice local eigenstate.

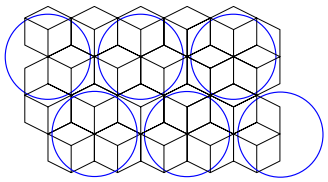

FIG. 10. (Color online) Nonoverlapping set of area units. Summing over type I states on these area units adds up to zero.

E. Another kagome model

Given the connection between frustrated geometry and flat bands (which we will elaborate on in the discussion), we examine one additional model—one inspired by Ref. 16 and mirroring its geometric structure. The magnetic model in Ref. 16 has been shown to support a spin liquid ground state. The magnetic model Hamiltonian consists of exchange interactions of equal strength on three different link types. This is described by an exchange matrix. We take this same matrix structure and construct a simple tight-binding model with it. The Hamiltonian is of the form

$$\mathcal{H} = \sum_{ij} c_i^\dagger t_{ij} c_j, \tag{12}$$

with the indices corresponding to the lattice sites of the kagome lattice. The hopping amplitudes are illustrated in Fig. 13 and we will refer to this hopping model as the kagome-3 model.

Our analysis finds that the band structure of this model consists of two degenerate flat bands at energy $\epsilon_0=+2t$ and one dispersive band $\epsilon_1=-t[4+2\Lambda(\mathbf{q})]$ with $\Lambda(\mathbf{q})$ the same function introduced in Eq. (3). The single dispersive band has a minimum energy of $-10t$ at $\mathbf{q}=0$ and a maximum energy of $-t$ at wave vector $\mathbf{q}=(4\pi/3)\hat{x}$ in our conventions. The flat bands are therefore *gapped* from the dispersive band with a gap of $\Delta=3t$.

Proceeding as for the other models in this paper, the localized states we find are illustrated in Fig. 15 and live on "bowtie" plaquettes. As in the pyrochlore lattice, naively there are three different "flavors" of bowtie plaquettes (and localized states). These can most easily be identified by considering how many bowties states involve a single up-

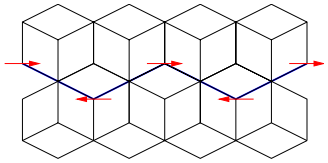

FIG. 11. (Color online) Noncontractible loop states. Only those sites with arrows on them have nonzero occupation.

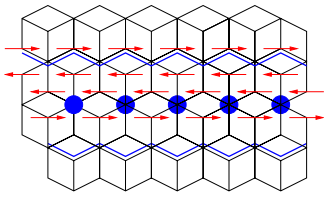

FIG. 12. (Color online) Sum of type II states (marked by filled circles at their centers) on a noncontractible strip of area units. Only those sites with arrows on them have nonzero occupation.

pointing triangle (corresponding to a unit cell). Were these states all linearly independent, we would have $3N$ states in the flat band rather than $2N$ (here as before, N is the number of unit cells). However, taking a bowtie plaquette state, rotating it around a hexagonal plaquette to produce six bowtie plaquette states around the hexagon (see Fig. 14), and finally summing these six wave functions produce zero. For each hexagonal plaquette, of which there are N, there is one such constraint and we find there are only two flavors of independent bowtie states—marked A, B in Fig. 15.

As in all the other examples we give in this paper, there are additional nonlocal constraints, which mandate the existence of noncontractible loop states. The constraints we find involve vanishing summations over the bowtie plaquette states of type A (see Fig. 15), with wave vectors $\mathbf{q} = \frac{1}{2}\mathbf{b}_2, \frac{1}{2}(\mathbf{b}_1+\mathbf{b}_2)$ (but not $\mathbf{q}=\frac{1}{2}\mathbf{b}_1$). Here $\mathbf{b}_{1,2}$ are the reciprocal-lattice vectors. In the exactly same manner, the sums over the type B plaquette states, with wave vectors $\mathbf{q} = \frac{1}{2}\mathbf{b}_1, \frac{1}{2}(\mathbf{b}_1+\mathbf{b}_2)$ (but not $\mathbf{q}=\frac{1}{2}\mathbf{b}_2$), also vanish. We therefore have four constraints and since there are a total of $2N$ flat-band states, we expect four noncontractible loop states to exist. These can easily be found graphically and are illustrated in Fig. 16.

As in Sec. III D, we find that in order for gapped flat bands to appear, we needed two different localized eigenstates occupying the same area unit as well as noncontractible loop states that are not associated with one of the two sets of local eigenstates.

IV. DISCUSSION

A. Summary

We have found that the presence or absence of band touchings can be understood for a variety of frustrated hopping models by a careful counting of linearly independent localized states. Crucial to this counting is the presence, which we found for all the models examined here, of noncontractible loop states. In all cases, a vanishing superposition of the localized states was found, always involving a sum over area patches that cover the entire lattice, but some with different weights in the summation (nonzero $\mathbf{q}$ for instance). When working in a toroidal geometry, for which momentum $\mathbf{q}$ remains a good quantum number, the missing states eliminated by this vanishing superposition were recovered as noncontractible loop states. The counting, for the case of a single flat band, is as follows. The total number of independent states with the flat-band energy is $N-M+dL$, where N is the number of unit cells, M is the number of localized-state-independent superpositions that vanish (the number of missing states), and L is the number of different flavors of noncontractible loop states for each of the d handles of the torus (in d dimensions). When this is larger than N, the flat band is degenerate with some other band at a finite number of points in momentum space.

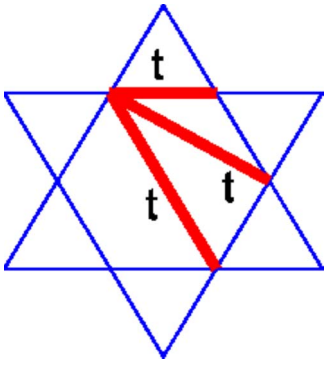

FIG. 13. (Color online) Tight-binding model with equal hopping amplitudes on three different link types.

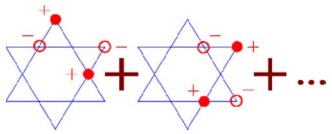

FIG. 14. (Color online) Illustration of the local constraint in the kagome-3 hopping model. Localized eigenstates living on the bowtie plaquettes are summed over the six plaquettes bordering a hexagonal plaquette in the kagome lattice. The figure shows two of these localized states with the correct relative phase needed for the summation to vanish. Only those sites with nonzero weight are denoted by (red) circles (filled for +1 and unfilled for −1).

B. Are frustrated hopping models frustrated?

We have referred to the hopping models discussed in this paper as frustrated, simply because (apart from the p-orbital honeycomb example) they reside on lattices exhibiting strong geometrical frustration for antiferromagnetism. It is interesting to see if this abuse of terminology has any truth to

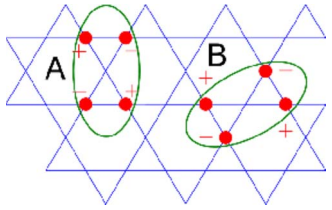

FIG. 15. (Color online) Localized eigenstates of the kagome-3 hopping model. The states have nonzero weight only on the four sites surrounding a bowtie plaquette (the encircled regions). The sites with nonzero weight are marked by filled (red) circles and with their relative signs indicated next to them. There are a number of different flavors of bowtie plaquettes (and localized states) −3 per unit cell. However there are only two independent bowtie states per unit cell. Here we show one choice of two independent bowtie states marked as A and B.

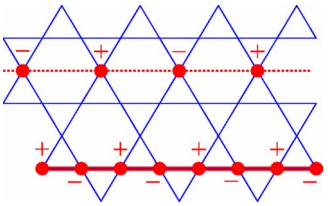

FIG. 16. (Color online) Noncontractible loop states of the kagome-3 model. There are two types of the noncontractible loops. One kind is the exactly same states appearing in the kagome model and is denoted by a continuous (red) path between the sites with nonzero weight. The other kind of noncontractible loop states are denoted by dashed line and consist of two sites with nonzero weight and alternating sign on each hexagonal plaquette in a chain of plaquettes.

it. Consider a general tight-binding Hamiltonian with a flat band

$$\mathcal{H} = -\sum_{ij} c_i^\dagger t_{ij} c_j, \tag{13}$$

where the indices i,j include all the generalized coordinates of the particles (position, orbital state, etc...). Choosing the particles to be fermionic and adding a spin $\frac{1}{2}$ index and an on-site interaction term, we have

$$\mathcal{H} = -\sum_{ij\alpha} c_{i\alpha}^\dagger t_{ij} c_{j\alpha} + U\sum_j c_{j\uparrow}^\dagger c_{j\uparrow} c_{j\downarrow}^\dagger c_{j\downarrow}. \tag{14}$$

Note that the interaction corresponds to the physical on-site repulsion only if the indices j represent only spatial coordinates, but this is only a minor complication we will ignore in this short and simplistic analysis.

At half filling of the fermions, for infinite repulsive U, we get a Mott insulating phase, with one fermion occupying each state of the (weighted) network of sites j described by the matrix t_{ij}. For finite but very large U, the virtual hopping of particles results in a Heisenberg model splitting the energy of the insulating states. It is very easy to show that the general Heisenberg model that emerges is

$$\mathcal{H} = \sum_{ij} J_{ij} \mathbf{S}_i \cdot \mathbf{S}_j + \mathcal{O}\left(\frac{t^3}{U^2}\right), \tag{15}$$

with $J_{ij}=4t_{ij}^2/U$, where $\mathbf{S}_j$ are the spin $\frac{1}{2}$ operators. The matrix structure that is responsible for the flat bands carries over to the exchange interaction matrix. In particular, if the hopping matrix takes on only two values, 0 and t, then $J_{ij}=(4t/U)t_{ij}$ and the matrices simply differ by a multiplicative factor.

When t_{ij} is nonzero for only nearest-neighbor sites i,j, the spin model "descending" from the hopping Hamiltonian is indeed geometrically frustrated. It is interesting to consider, however, a possibly more direct connection between flat bands and frustration. Indeed, somewhat rough arguments suggest that, fairly generally, the classical spin Hamiltonian with exchange $J_{ij}=(4t/U)t_{ij}$ has an extensive ground-state degeneracy when the lowest-energy eigenstates of t_{ij} form a flat band. We discuss some additional conditions below.

The connection between flat bands and ground-state degeneracy is through the Luttinger-Tisza method for finding ground states of classical spin models. The idea is the following. We first trade the normalization constraint on the spins $|\mathbf{S}_j|=S$ for the weaker condition

$$\sum_j |\mathbf{S}_j|^2 = N_s S^2, \tag{16}$$

where N_s is the number of spins. With this weaker constraint, it is simple to minimize $\mathcal{H}$ in Eq. (15). This is guaranteed to give an energy which is at least as low as for the minima of $\mathcal{H}$ taking proper spin normalization into account. The general solution is an arbitrary real linear combination of the minimum-energy eigenstates of $J_{i,j}$ and hence of $t_{i,j}$. Because the hopping matrix is real, the eigenstates may also be chosen real. When there are n_f flat bands, there are a total of $n_f N$ such eigenstates with minimum energy for a lattice containing N unit cells. The solution is

$$\mathbf{S}_j = \sum_{a=1}^{Nn_f} \mathbf{s}_a \phi_j(a), \tag{17}$$

where $\phi_j(a)$ is the ath eigenstate of t_{ij} and $\mathbf{s}_a$ is an unknown vector of real coefficients for each a. The total number of variables that may be varied is then three real numbers for each a and hence $3Nn_f$ real numbers. Now we can attempt to impose the necessary constraints to get a physical minimum for the classical spin model. These consist of one constraint per spin on the spin magnitude. If the lattice contains n_b spins in its basis (i.e., sites in the unit cell), then this gives Nn_b constraints. Subtracting the number of constraints from the number of variables gives a total of $(3n_f-n_b)N$ degrees of freedom remaining for physical minima of the classical spin model. Thus, for $n_b<3n_f$, we are led to expect an extensive degeneracy (macroscopic entropy) of spin ground states. This counting is certainly crude, and since the normalization constraints are nonlinear, not entirely rigorous. For instance, if $n_b=3n_f$, it is probably the case that extensive ground-state entropy may or may not be present, depending on other details of the model. This is born out, for instance, by the case of the nearest-neighbor kagome model, for which there is indeed an extensive ground-state entropy, while $n_b=3, n_f=1$. However, we believe the conclusion provides a reasonable qualitative guide, although the estimate of the entropy density is probably unreliable. Thus a large U Hubbard model with a kinetic energy and with flat maximum energy bands indeed, when $n_b<3n_f$, exhibits macroscopic ground-state entropy, the classic signature of frustration.

C. For the future

The discussion in this paper is only a prelude to the study of interacting bosons and fermions in flat-band systems. When the flat band is at very low-filling (low density of particles) short-range interactions of arbitrary (weak or strong) strength lead to particle localization into a variety of crystalline patterns that are model specific.[10–15,17] When interactions have finite range and are repulsive, multiple particles can be present in spatially separated localized states

with zero interaction cost, and the corresponding many-body wave function remains a many-body eigenstate. If the flat band has the minimum kinetic energy, such a state minimizes simultaneously the kinetic and interaction energy and is therefore a ground state. Such states are generically possible for particle densities below some "close-packing" threshold, at which interaction cost becomes inevitable. The states precisely at this threshold density are usually (but not always) periodic crystalline configurations and are analogous to the Wigner crystal states of electrons in the lowest Landau level (LLL).

In the case of electrons in the LLL, the more interesting fractional quantum Hall states occur *above* this filling factor when there is some unavoidable interaction cost. However, because of the presence of a (large) gap between the LLL and the first Landau level, the interactions act entirely within the former. The zoo of fractional quantum Hall states is understood primarily from studies of the Coulomb interaction *projected* into the LLL subspace. A very interesting question is whether any similar richness of behavior might occur above the close-packing threshold when interactions are included in the frustrated hopping models discussed here. This would appear a promising place to search for exotic orderless quantum spin liquid phases, loosely analogous to fractional quantum Hall liquids, that have been hypothesized to occur, e.g., in frustrated magnets.[18,19]

How to attack the problem in the range of densities, for which the particles can still be accommodated in the flat band(s) but above close packing, is an interesting open problem. A first step might be to try and project the Hilbert space onto the flat band. At this point the band touchings re-enter the picture as a *hindrance* to this search. Projection of the Hamiltonian into the lowest-energy flat band is strictly controlled only when there is a gap between this band and the higher dispersive ones and when this gap is large compared to the strength of interactions.

It is intriguing to speculate that liquid states in this regime, at least for weak interactions, may have unconventional properties. With the increasing accessibility of such Hamiltonians in ultracold atomic systems in optical lattices, clarification of this regime may well come experimentally rather than theoretically.

ACKNOWLEDGMENTS

The authors would like to acknowledge Sankar Das-Sarma for early collaboration on related work and John Chalker for the illuminating discussions. L.B. was supported by the Packard Foundation and the National Science Foundation through Grant No. DMR04-57440, and in part by NSF Grant No. PHY05-51164. C.W. was supported by the Sloan Research Foundation, ARO Grant No. W911NF0810291, NSF Grant No. DMR-0804775, the start-up funding at UCSD, and Academic Senate at UCSD.

[1] C. Herring, Phys. Rev. **52**, 365 (1937).
[2] A. Geim and K. Novoselov, Nat. Mater. **6**, 183 (2007).
[3] D. Hofstadter, Phys. Rev. B **14**, 2239 (1976).
[4] S. Murakami, New J. Phys. **9**, 356 (2007).
[5] J. L. Manes, F. Guinea, and M. A. H. Vozmediano, Phys. Rev. B **75**, 155424 (2007).
[6] A. Mielke, J. Phys. A **25**, 4335 (1992).
[7] H. Tasaki, Prog. Theor. Phys. **99**, 489 (1998).
[8] S. Nishino, M. Goda, and K. Kusakabe, J. Phys. Soc. Jpn. **72**, 2015 (2003).
[9] O. Derzhko, A. Honecker, and J. Richter, Phys. Rev. B **76**, 220402 (2007).
[10] J. Schulenburg, A. Honecker, J. Schnack, J. Richter, and H.-J. Schmidt, Phys. Rev. Lett. **88**, 167207 (2002).
[11] M. E. Zhitomirsky and H. Tsunetsugu, Prog. Theor. Phys. **160**, 361 (2005).
[12] O. Derzhko, J. Richter, A. Honecker, and H.-J. Schmidt, Low Temp. Phys. **33**, 745 (2007).
[13] H.-J. Schmidt, J. Richter, and R. Moessner, J. Phys. A **39**, 10673 (2006).
[14] M. E. Zhitomirsky and H. Tsunetsugu, Phys. Rev. B **75**, 224416 (2007).
[15] C. Wu, D. Bergman, L. Balents, and S. Das Sarma, Phys. Rev. Lett. **99**, 070401 (2007).
[16] L. Balents, M. P. A. Fisher, and S. M. Girvin, Phys. Rev. B **65**, 224412 (2002).
[17] O. Derzhko and J. Richter, Phys. Rev. B **70**, 104415 (2004).
[18] P. W. Anderson, Mater. Res. Bull. **8**, 153 (1973).
[19] P. Fazekas and P. W. Anderson, Philos. Mag. **30**, 423 (1974).